3D LASER PULSE SHAPING, MEASUREMENT, AND 3D ELECTRON BEAM PROFILE MEASUREMNT FOR PHOTOINJECTORS

Yuelin Li, ANL, Argonne, IL 60439, U.S.A.

Abstract

We propose a schem of shaping laser pulses in 3D exploiting chromatic aberration and laser phase tailoring. We demonstrated a interferometry method of measuring 3D distribution of a laser pulse. For the electron beam diagnostics, a non interceptive time resolved laser wire scheme is proposed using a ultrafast laser pulse in a line focus to scatter from the beam under consideration. By imaging the scattered photons at different delays between the laser and the beam, the 3D distribution can be reconstructed.

INTRUDCUTION

For high brightness photoinjectors, it is critical to be able to shape the 3D form of the drive laser pulse, to understand its actual 3D distribution, and the initial electron beam in order to properly compensate the emittance growth [1, 2].

We propose a 3D pulse shaping scheme which can be potentially used to generate 3D uniform ellipsoidal beam [3]. In a proof of principle experiment [4, 5], we demonstrated that the shaping method and at the same time developed a method for measuring the 3D distribution of a laser pulse based on a crossing interferometer. We also propose to use a time-resolved laser wire to measure the 3D distribution of a low energy electron beam, e.g., one that is leaving a photoinjector, based on imaging the photons scattered from the electron beam from a ultrafast laser pulse.

3D LASER PULSE SHAPING

To shape the laser pulse in 3D, we exploit the chromatic aberration effect in an optical lens. The dependence of the refractive index upon the optical frequency gives rise to the chromatic aberration in a lens, where the change of the focal length due to a shift in frequency $\delta\omega$ is

$$\delta f = -\frac{f_0}{n_0 - 1}\chi\delta\omega,\qquad(1)$$

where f_0 is the nominal focal length at ω_0. We assume a constant $\chi = dn/d\omega$ for this analysis. For a Gaussian beam, the beam size at the nominal focal plane is

$$w \approx w_0\left[1 + (\delta f / z_R)^2\right]^{1/2}.\qquad(2)$$

Here $w_0 = N\lambda_0/\pi$ is the beam waist at the nominal wavelength λ_0, with N the numerical aperture, and $z_R = \pi w_0^2/\lambda_0$ is the Rayleigh range. It is obvious, therefore, if one can program $\delta\omega$ in time, a time-dependent beam size can be achieved. At $\delta f \gg z_R$, one has $w(t) \cong |\delta f(t)|/N$, thus the phase of the laser pulse is

$$\phi(t) = \pm\int\delta\omega(t)dt = \pm\frac{n_0 - 1}{\chi}\frac{N}{f_0}\int w(t)dt \cdot\qquad(3)$$

For a desired time-dependent intensity $I(t)$, the amplitude of the laser should be

$$A(t) \propto I(t)^{1/2}w(t)\cdot\qquad(4)$$

As an example, to generate an ellipsoidal radial envelop with maximum radius of R and full length of $2T$, the transverse beam size as a function of time is $w(t) = R[1 - (t/T)^2]^{1/2}$. Using Eq. (3), this in turn gives the phase,

$$\phi(t) = -\omega_0 t \pm \frac{\Delta\omega}{2}\left[t\left(1 - \left(\frac{t}{T}\right)^2\right)^{\alpha} + T\sin^{-1}\frac{t}{T}\right],\qquad(5)$$

where $\alpha = 1/2$, and $\Delta\omega = (n_0-1)NR/\chi f_0$ is the maximum frequency shift. To keep the laser flux $|A(t)|^2/w(t)^2$ constant over time, we have

$$A(t) = A_0\left[1 - \left(\frac{t}{T}\right)^2\right]^{\eta},\qquad(6)$$

with $\eta = 1/2$. Equations (4) and (5) describe a pulse that can form a spatiotemporal ellipsoid at the focus of the a lens. In particle tracking simulations, the performed of so generated ellipsoidal beam give excellent emittance performance [3, 5].

3D LASER PULSE MEASURMENT

Method

The scheme is based on the interference between the drive laser pulse and a short interrogation pulse. The schematic of the experiment is shown in Fig. 1. Assuming that the interrogation (probing) laser and the main laser pulse has a field distribution as $A_{p, m}(t, r)$, the interference pattern on the detector is:

$$I(r) = I_m(r) + I_p(r) + 2\cos(\omega[\tau + \delta(r)])\times$$
$$\int A_m(t,r)A_p(t - \delta(r) - \tau, r)\cos[\phi_m(t) - \phi_p(t - \delta(r) - \tau)]dt,\qquad(7)$$

where

$$I(r) = \int|A(t,r)|^2 dt,\qquad(8)$$

is the integrated intensity and $\phi(t)$ is the phase of the laser beams; the subscripts m and p denote the main and probe beam, respectively; τ is the timing delay and $\delta(r)$ is the additional location dependent delay due to the angle between the two beams, respectively. The phase term in the integral, though impossible to evaluate for each location, only causes the interference fringes at the detector to shift. Therefore, if the probe pulse is much shorter than the main pulse, Eq. (7) can be reduced to
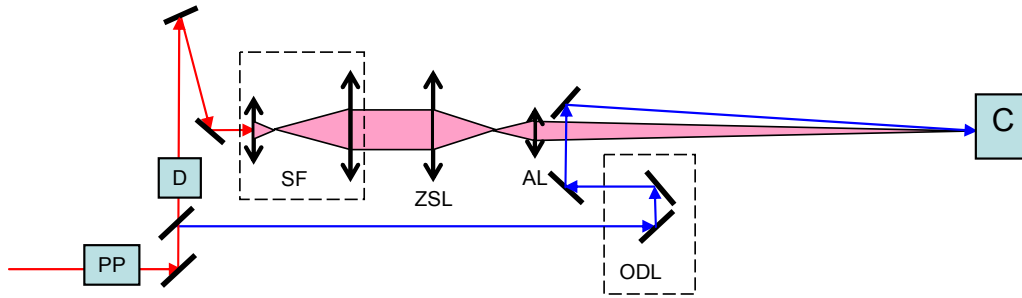
Figure 1: Schematic of the experiment for the 3D laser pulse profile measurement. Keys: PP: pulse picker; D: AOPDF; SF: achromatic spatial filter; ZSL: ZnSe lens; AL: achromatic image relay lens; ODL: optical delay line; C: camera.

$$I(\mathbf{r}) \approx I_m(\mathbf{r}) + I_p(\mathbf{r}) + 2\cos\left(\omega[\tau + \delta(\mathbf{r})]\right)\sqrt{\Delta t_p i_m(\tau, \mathbf{r})}\sqrt{I_p(\mathbf{r})}. \quad (9)$$

Here Δt_p is the duration of the probe pulse, and

$$i(\tau, \mathbf{r}) = |A(\tau, \mathbf{r})|^2 \quad (10)$$

is the time-dependent intensity distribution. The second term in Eq. (9) describes the fringes as functions of delay and location, from which one can extract the contrast ratio $R(\tau, \mathbf{r})$, which in turn gives

$$i_m(\tau, \mathbf{r}) \propto R^2(\tau, \mathbf{r}) / I_p(\mathbf{r}). \quad (11)$$

Experiment Results

In the proof-of-principle experiment, the spatiotemporal distribution of a laser pulse shaped in 3D is measured [4, 5]. The pulse is shaped according to Eqs. (5, 6), using a combination of a lens with chromatic aberration and an acousto-optic programmable dispersive filter (AOPDF) which imposes the phase and amplitude on to the pulse. The main laser pulse has a full width of 2 ps and the probe pulse of 130 fs. The main pulse is spatially filtered to generate a Gaussian beam using a pair of achromatic lenses and a pinhole. A plano-spherical ZnSe lens (25-

mm diameter, 88.9-mm radius of curvature, and 2.9-mm center thickness, Janos Technology, A1204-105) is used for its high dispersion (250 fs^2/mm at 800 nm) to form the desired spatiotemporal distribution at its focal plane. The focal plane is image-relayed by an achromatic lens onto a CCD camera to interfere with the probe beam. The interference fringes as a function of delay between the two beams are recorded on a 12-bit camera and are used to extract the spatiotemporal intensity distribution of the main beam according to Eqs. (7-11). The result of the 3D measurement is given in Fig. 2, where the measured spatiotemporal distribution is compared with that from a numerical simulation under different conditions.

The experiment shows that the method of shaping works in principle. It also shows the time resolved interferometer is very useful for measuring spatiotemporal structures of a laser pulse. The structures in the pulse are mostly due to diffraction, which is more prominent at lower beam aperture. At large apertures, these structures smooth out, as can be seen in Fig. 2, right column. Overall, the measurement shows good agreement with the Fourier optics simulation [4, 5].
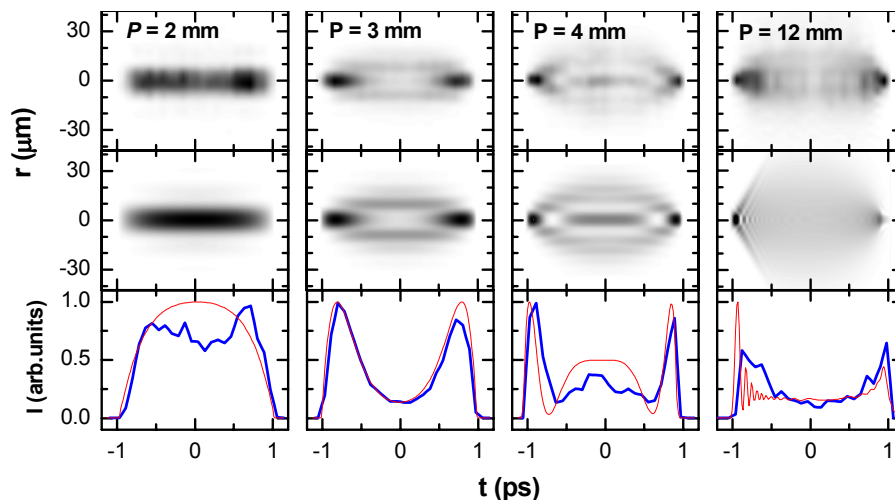

Figure 2: Measured (upper row) and simulated (middle row) spatiotemporal intensity distribution with different iris radius P using the experiment condition. The iris is located in front of the ZnSe lens in Figure 1. The low row shows comparison of the intensity at r=0 extracted from the upper and middle rows.

METHOD FOR 3D ELECTRON BEAM PROFILE MEASUREMENT

Method

Even the laser pulse shape is fully characterized, the electron beam can still take a form different form the laser pulse shape. To measure the 3D shape of the beam, we propose a time resolved laser wire, shown in Fig. 3. A line-focused femtosecond laser pulse intersects an electron beam at 90 degree. As the laser interacts with the electrons in the beam, photons are scatter off the electrons and propagate in a cone following the electron propagation direction. The photons are collected and imaged by a proper mirror onto a 2-D area detector. As the total radiation is proportional to the local electron density, at a fixed delay, the image is a skewed time slice of the electron density distribution. By changing the delay between the laser pulse and the electron beam, a series of images are collected and can be used to reconstruct the 3D density distribution.

Assume a laser profile with a known 3 D Gaussian distribution $n_p(x, y-c(t-\tau), z)$ propagating the y direction,

$$n_p(x,y,z,t) = \frac{N_p}{(2\pi)^{3/2}\sigma_x\sigma_z\sigma_t}\exp\left[-\frac{x^2}{2\sigma_x^2}-\frac{z^2}{2\sigma_z^2}-\frac{(y-ct)^2}{2\sigma_t^2}\right],$$
(13)

where σ is the root mean square (rms) size, N_p is the total number of photons. The electron beam has energy of γ and an unknown 3-D density distribution,

$$n_e(x,y,z) = N_e f[x,y,z-v_z(\tau-t)]$$
(14)

propagating in the z direction at a speed of v_z, with τ the delay between the electron beam and the laser beam. Here f is the normalized density distribution function, N_e is the total number of electrons. If we set the interaction point at $z=0$, the number of scattered photons as a function of (x, y) at a particular τ can be expressed as,

$$n_s(x,y,\tau) = \Sigma_t N_e \iint_{t,z} f[x,y,z-v_z(\tau-t)]n_p(x,y,z,t)dtdz \cdot$$
(15)

Here $\Sigma_t = 8\times10^{-26}$ cm^2 is the Thomson scattering cross section. Set

$$\overline{f[x,y,-v_z(\tau-t)]} = \frac{1}{\delta}\int_\delta f[x,y,-v_z(\tau-t)]dt,$$
(16)

With

$$\delta = \sqrt{2\pi}\sqrt{\sigma_z^2+(v_z\sigma_t)^2}\cdot$$
(17)

The integration in Eq. (15) can be approximated by the following

$$n_s(x,y,\tau) \approx \Sigma_t N_e \overline{f\left[x,y,-v_z\left(\tau-\frac{y}{c}\right)\right]}\frac{N_p}{\sqrt{2\pi}\sigma_x}\exp\left(-\frac{x^2}{2\sigma_x^2}\right)\cdot$$
(18)

The term on the left hand side can be recorded on a camera via imaging optics and from which the beam distribution with a resolution in longitudinal dimension of δ can be retrieved:

$$\overline{f\left[x,y,v_z\left(\frac{y}{c}-\tau\right)\right]} \propto n_s(x,y,\tau)\exp\left(\frac{x^2}{2\sigma_x^2}\right).$$
(19)

Eq. (19) is a 2D electron density profile at delay τ slanted at an angle of v_z/c in the y-z plain. The 3 D profile of the beam can be reconstructed by changing the delay τ to cover the whole beam a longitudinal resolution of δ.

Technical Feasibility

To estimate the number of scattered photons, without losing generality, we assume a 3D Gaussian beam profile,
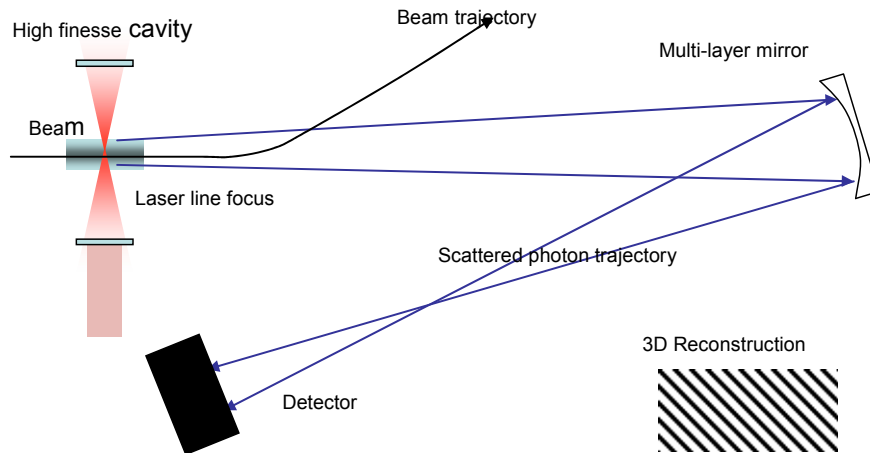

Figure 3: Top view of the schematic of the time-resolved laser wire concept. A laser pulse is stored in a high-finesse resonator cavity with a high aspect ratio elliptic beam at the center. The line focus of the laser is perpendicular to the paper. The electron beam propagates from the left and after the interaction is deflected by a bending magnet. The scatter photons are collected by a multilayer mirror and imaged on a area detector. Each image at a delay is a schewed slice of the 2 D distribution of the beam, which can be used to reconstruct the 3 D beam profile illustrated in the lower right corner, also a top view corresponding to the view of the schematic.

$$f(x,y,z) = \frac{1}{(2\pi)^{3/2}\sigma_x^2\rho_z}\exp\left[-\frac{x^2}{2\sigma_x^2}-\frac{y^2}{2\sigma_x^2}-\frac{(z-v_zt)^2}{2\rho_z^2}\right], \quad (20)$$

with a beam rms radius matched to the length of the laser line focus σ_x. Equation (18) can be now written as:

$$n_s(x,y,\tau) \approx \Sigma_t \frac{N_eN_p}{(2\pi)^2\sigma_x^3\rho_z}\exp\left[-\frac{x^2}{\sigma_x^2}-\frac{y^2}{2\sigma_x^2}-\frac{[v_z(y/c-\tau)]^2}{2\rho_z^2}\right]. \quad (21)$$

Thus the total number of scattered photon per interaction can be approximated as,

$$n_s(\tau) = \iint_{x,y} n_s(x,y,\tau)dxdy$$
$$\approx \Sigma_t \frac{N_eN_p}{2\sqrt{2\pi}\sigma_x\rho_z}\exp\left(-\frac{\tau^2}{2\rho_z^2}\right) \quad (22)$$

Here we assume that the z-variation of the distribution is small when the laser pulse propagates across the beam. With a repetition rate of the laser and beam at F and a laser accumulating cavity with a quality factor of Q, the total photon number per second at zero delay is

$$N_s(0) = QFn_s(0) \approx QF\Sigma_t \frac{N_eN_p}{2\sqrt{2\pi}\sigma_x\rho_z}. \quad (23)$$

For a typical beam condition for an ERL DC photo injector [6], let $\sigma_x = 0.5$ mm and bunch length $\rho_z/v_z = 20$ ps, and total charge of 100 pC, i.e., $N_e = 6.25\times10^8$, and a system repetition rate $F = 100$ MHz. With 5 nJ per laser pulse at 800 nm, a per pulse photon number $N_p = 2\times10^9$ (an average power of 0.5 W, a laser of this performance is off the shelf product of many commercial vendors), we have from Eq. (22) the total scattered photon number per interaction at zero delay of 4×10^{-7}. With $F = 100$ MHz, this gives about 40 photons per second.

To further booster the photon number, a high-finesse passive optical cavity can be used to accumulate the laser pulse with a quality factor of $Q = 10^4$ by another factor of about 10^4, as has been proposed for several Thomson scattering x-ray sources [7]. This will give about 4×10^5 photons per second. In the current case, a highly elliptical beam (line focus) is needed in the resonator cavity, such asymmetric resonant cavities have been widely applied end-pumped diode laser systems where the diode pump beam is focused to line at the lasing medium [8].

To image the x-ray, it is important to be very efficient. A spherical or a paraboloidal multilayer mirror can be used to collect the light and image it onto a detector. Assuming the beam energy at about 5 MeV ($\gamma = 10$), the scattered photon energy is:

$$E = E_L \frac{2\gamma^2}{1+\gamma^2\theta^2}(1-\cos\phi) \quad (24)$$

Where $\phi = 90$ degree is the crossing angle. And the differential cross section is

$$\frac{d\Sigma_t}{d\theta} \propto \frac{1+\gamma^4\theta^4}{(1+\gamma^2\theta^2)^2}\theta. \quad (25)$$

It has a maximum at $\theta \cong 0.4/\gamma$, where the photon energy is $E = 1.72\ \gamma^2\ E_L$. For the above beam energy $\gamma = 10$, we have the peak photon energy at $E = 266$ eV. This is in the soft x-ray range, where multilayer coatings with near-normal incidence reflectance of 20% has been
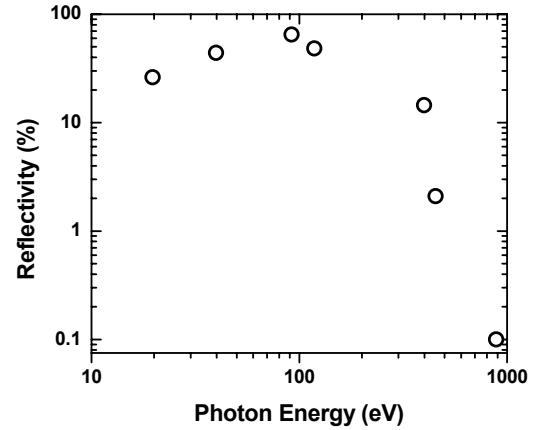

Figure 4: Best near normal incidence reflectance efficiency of multilayer mirrors as a function of photon energy. From lower to high energies, the data are adapted from refs. [9-15], respectively.

demonstrated and higher efficiency is expected with oblique incidence angles, and with improved design and fabrication procedure [9-15]. Figure 4 is a summary of the best experiment measured reflectance for multilayer mirrors from 10 to 1000 eV.

Finally, for the area detector, a back-side illuminated CCD camera, with a quantum efficiency of close to 80-90% at 266 eV [16] can be used. Using the CCD parameters in ref. [16] and the mirror efficiency, the total expected counts is about 4×10^5 per image for an integration time of one second. Of course, other high efficiency device can also be used for this purpose.

With high quality imaging system, the spatial resolution is only limited by the pixel size of the detector. The temporal resolution is limited by the line focus width of the laser and the pulse duration as expressed in Eq. (17). The temporal resolution is, in addition, also limited by the timing jitter of the between the beam and the laser, which can be well under 100 fs.

Though we limited our discussion to a low energy beam, the scheme can also be used at higher beam energy with proper imaging and detector systems. The potential difficulty as one move to high beam energy is the scaling of the scattered photon energy quickly to hard x-ray, where the efficiency of multilayer mirrors almost diminishes (see Fig. 4) although at larger off normal incidence angles the reflectance can be greatly enhanced. Although higher laser power can be part of the solution, an optimized design can take fully advance of the current advances in x-ray optics development for an efficient imaging system.

To move the scattered photon energy to lower region suitable for imaging optics, smaller crossing angle can be used as shown in Eq. (24). However, the total photon number will also be reduced by a factor of $(1-\cos\phi)$ [16].

CONCLUSION

A 3D laser pulse shaping scheme potentially useful for 3D uniform ellipsoidal beam generation is proposed and demonstrated in a proof-of principle experiment. In the experiment, a cross interferometer is developed for spatiotemporal shape measurement of the pulse. We also propose a time resolved laser wire system for 3 D electron beam profile measurement and discussed it technical feasibility.

REFERENCES

[1] B. E. Carlsten, Nucl. Instrum. Methods A **285**, 313 (1989);

[2] L. Serafini and J. B. Rosenzweig, Phys. Rev. E **55**, 7565 (1997).

[3] Y. Li, and J. W. Lewellen, Phys. Rev. Lett. **100**, 074801 (2008).

[4] Y. Li and S. Chemerisov, Opt. Lett. **33**, 1996 (2008).

[5] Y. Li, S. Chemerisov, and J. Lewellen, Phys. Rev. ST Accel. Beams 12, 020702 (2009).

[6]   I. V. Bazarov and C. K. Sinclair, Phys. Rev. ST Accel. Beams 8, 034202 (2005)

[7] W.S. Graves, W. Brown, F.X. Kaertner and D.E. Moncton, Nucl. Instrum. Methods Phys. Research A, in press.

[8] F. Krausz, J. Zehetner, T. Brabec and E. Winter, Opt. Lett. 16, 1496 (1991); and references therein.

[9] B. Kjornrattanawanich, D. L. Windt, and J. F. Seely, Opt. Lett. 33, 965-967 (2008).

[10] T. Ejima, A. Yamazaki, T. Banse, K. Saito, Y. Kondo, S. Ichimaru, and H. Takenaka, Appl. Opt. 44, 5446-5453 (2005).

[11] C. Montcalm, R. F. Grabner, R. M. Hudyma, M. A. Schmidt, E. Spiller, C. C. Walton, M. Wedowski, and J. A. Folta, Appl. Opt. 41, 3262-3269 (2002).

[12] B. Sae-Lao and C. Montcalm, Opt. Lett. 26, 468-470 (2001).

[13] F. Eriksson, G. A. Johansson, H. M. Hertz, E. M. Gullikson, U. Kreissig, and J. Birch, Opt. Lett. 28, 2494 (2003).

[14] N. Ghafoor, P. O. Å. Persson, J. Birch, F. Eriksson, and F. Schäfers, Appl. Opt. 45, 137 (2006).

[15] D. L. Windt, E. M. Gullikson, and C. C. Walton, Opt. Lett. 27, 2212 (2002).

[16] Y. Li, Z. Huang, M. D. Borland, and S. Milton, Phys Rev ST AB 5, 044701 (2002) and references therein.

.